Earthq Eng & Eng Vib (2017) 16: 365-382 **DOI**:10.1007/s11803-017-0387-8

Seismic response evaluation of base-isolated reinforced concrete buildings under bidirectional excitation

Satish Bhagat† and Anil C. Wijeyewickrema‡

Department of Civil and Environmental Engineering, Tokyo Institute of Technology, Tokyo 152-8552, Japan

Abstract: This paper reports on an investigation of the seismic response of base-isolated reinforced concrete buildings, which considers various isolation system parameters under bidirectional near-fault and far-fault motions. Three-dimensional models of 4-, 8-, and 12-story base-isolated buildings with nonlinear effects in the isolation system and the superstructure are investigated, and nonlinear response history analysis is carried out. The bounding values of isolation system properties that incorporate the aging effect of isolators are also taken into account, as is the current state of practice in the design and analysis of base-isolated buildings. The response indicators of the buildings are studied for near-fault and far-fault motions weight-scaled to represent the design earthquake (DE) level and the risk-targeted maximum considered earthquake (MCE_R) level. Results of the nonlinear response history analyses indicate no structural damage under DE-level motions for near-fault and far-fault motions and for MCE_R-level far-fault motions, whereas minor structural damage is observed under MCE_R-level near-fault motions. Results of the base-isolated buildings are compared with their fixed-base counterparts. Significant reduction of the superstructure response of the 12-story base-isolated building compared to the fixed-base condition indicates that base isolation can be effectively used in taller buildings to enhance performance. Additionally, the applicability of a rigid superstructure to predict the isolator displacement demand is also investigated. It is found that the isolator displacements can be estimated accurately using a rigid body model for the superstructure for the buildings considered.

Keywords: base isolation; bidirectional excitation; bounding analysis; far-fault ground motion; near-fault ground motion; nonlinear analysis

1 Introduction

Base isolation improves the seismic performance of buildings by reducing inter-story drifts, floor accelerations, and story shear forces in the superstructure (Naeim and Kelly, 1999; Okamoto *et al.*, 2002; Tsai *et al*., 2004). Base isolation works by shifting the fundamental period of the building beyond the dominant periods of ground motions, and increasing the energy dissipation capability with the use of isolators between the super- and sub-structures. During seismic events the base-isolated superstructure is expected to have negligible inelastic deformation since most of the energy is dissipated at the isolation level, resulting in superior performance of the building.

Most of the previous studies on base-isolated buildings are based on simplified modeling approaches such as: (i) single-degree-of-freedom (SDF) systems (Jangid and Kelly, 2000, 2001; Fadi and Constantinou, 2010, Mahmoud *et al*., 2012; Pant *et al*., 2013a); (ii) two-degree-of-freedom (two-DOF) systems (Ordonez *et al*., 2003; Panchal and Jangid, 2008; Sayani and Ryan, 2009; Mahmoud and Gutub, 2013); (iii) multi-degree-of-freedom (MDF) lumped mass models (Hall *et al.*, 1995; Alhan and Gavin, 2004; Matsagar and Jangid, 2004; Ariga *et al.*, 2006; Ye *et al*., 2009; Becker and Mahin, 2013; Chimamphant and Kasai, 2016; Oliveira *et al.*, 2015); and (iv) two-dimensional models (Mazza and Vulcano, 2009, 2012; Ribakov, 2010; Calugaru and Panagiotou, 2014). Although these models of base-isolated buildings are easy to implement, the seismic response obtained may not represent the real behavior of the superstructure (Alhan and Sürmeli, 2011). Hence, it is necessary to use a three-dimensional (3D) modeling approach to simulate the actual behavior of the superstructure during seismic events. Previous studies considering 3D models of base-isolated buildings include the work of Nagarajaiah *et al*. (1991), Providakis (2008a, b), Sorace and Terenzi (2008, 2014), Kilar and Koren (2009), Alhan and Sürmeli (2011), Di Sarno *et al*. (2011), Ozdemir and Akyuz (2012), Pant and Wijeyewickrema (2013, 2014), Varnava and Komodromos (2013), Castaldo *et al*. (2015), Masroor and Mosqueda (2015). These studies

Correspondence to: Anil C. Wijeyewickrema, Department of Civil Engineering, Tokyo Institute of Technology, 2-12-1 O-okayama, Meguro-ku, Tokyo 152-8552, Japan
Tel: +81-3-5734-2595; Fax: +81-3-5734-3578
E-mail: wijeyewickrema.a.aa@m.titech.ac.jp
†PhD candidate; ‡Associate Professor
Received January 20, 2016; **Accepted** June 13, 2016

have considered buildings up to 8-stories, with a few of them considering nonlinearities in the superstructure and the isolation system.

Near-fault motions, containing long period velocity pulses, have been a major concern in the analysis of base-isolated structures, as these ground motions result in large response in both the superstructure and the isolation system. These ground motions have the potential of causing nonlinear deformations in the superstructure, especially for shaking beyond design-level earthquakes. Jangid and Kelly (2001) investigated the effects of near-fault motion on a single-story base-isolated building and showed that these ground motions can increase the base displacement at longer isolation periods. Mazza and Vulcano (2009, 2012) studied the effects of near-fault motion on a 5-story base-isolated building and concluded that the near-fault motions with pulse-like characteristics can induce unexpected ductility demands on the girders and columns at the lower stories. Pant and Wijeyewickrema (2014) compared the seismic performance of a 4-story base-isolated building under far-fault non-pulse-like motions and near-fault pulse-like motions and showed that near-fault motions induce larger demands in the isolation system as well as the superstructure. However, note that Jangid and Kelly (2001) and Mazza and Vulcano (2009, 2012) did not consider far-fault motions in their analyses.

The effect of bidirectional excitation on the response of base-isolated structures has been considered previously by Jangid and Kelly (2001), Tena-Colunga and Pérez-Osornio (2006), Alhan and Sürmeli (2011), Ozdemir and Akyuz (2012), Pant and Wijeyewickrema (2014). In most of these studies which focus on the response of the isolation system, the superstructure is assumed to be either rigid or linear elastic, although Pant and Wijeyewickrema (2014) who investigated seismic pounding of a RC building with retaining walls, considered the nonlinear behavior of the superstructure and the isolation system.

According to the current state of practice for elastomeric bearing systems, bounding values of isolator properties that account for variations in material properties of the bearing during the time of manufacture and the changes in mechanical properties over the installed lifetime must be addressed by the design (ASCE, 2010; Kalpakidis *et al*., 2010; Pant and Wijeyewickrema, 2014). The equivalent lateral force (ELF) method of ASCE 7-10 (ASCE, 2010) estimates the isolation system displacement demands based on the lower bound (LB) properties, whereas forces transmitted to the superstructure are based on the upper bound (UB) properties. The response history analysis for the design verification of a base-isolated building must be carried out using both the LB and UB properties of isolators, although most research studies have not considered these bounding values.

In the present study, the seismic performance of base-isolated RC buildings under bidirectional near-fault motions and far-fault motions is investigated, by carrying out 3D finite element analyses considering material and geometric nonlinearities using the LB and UB properties of the isolation system. Nonlinear response history analysis is carried out for near-fault motions and far-fault motions, scaled to represent both the design earthquake (DE) and risk-targeted maximum considered earthquake (MCE_R). The response of base-isolated superstructure is discussed in terms of inter-story drift ratio, normalized story shear force, and floor acceleration. Next, nonlinear response history analysis of the buildings with a fixed-base condition is performed and the response compared with the performance of the base-isolated buildings. In addition, the applicability of using a rigid superstructure to predict the isolator displacement demand is also discussed.

2 Building description and design

In this study, 4-, 8-, and 12-story base-isolated RC moment-frame buildings are considered. The buildings are symmetric with coinciding center of mass and center of stiffness and are 3-bay by 3-bay. The bay width is 6.0 m in both directions and each story is 4.0 m in height, except the first story which is 4.5 m high as shown in Fig. 1. The buildings were designed using the modal response spectrum method, following the provisions of International Building Code (ICC, 2012), ASCE 7-10 (ASCE, 2010), and ACI 318-11 (ACI, 2011). SAP2000 (2013) was used in the design and the 100% X + 30% Y of the lateral force combination was used. The design response spectrum was constructed for an arbitrary location in California described by coordinates 33.75 N, 117.9 W and the soil is considered to be stiff soil (Site Class D). The buildings are intended to be used as office buildings (Risk Category III). The mapped MCE_R spectral response acceleration parameters are S_s = 1.447 g and S_1 = 0.532 g at short periods and 1-s period, respectively. Based on the site class, design spectral accelerations and risk category, the building is determined to be under seismic design category D and the special moment frame system was selected for the superstructure. The superstructure was designed for forces associated with DE whereas the isolation system was designed for the effects of MCE_R. The compressive strength of concrete is 28 MPa and the yield strengths for main steel reinforcement bars and ties are 420 MPa and 300 MPa, respectively. Beam and column section details are shown in Table 1 and Table 2, respectively. A slab thickness of 200 mm is taken for all the floors. Dead load consists of member self-weight, and 7.8 kN/m and

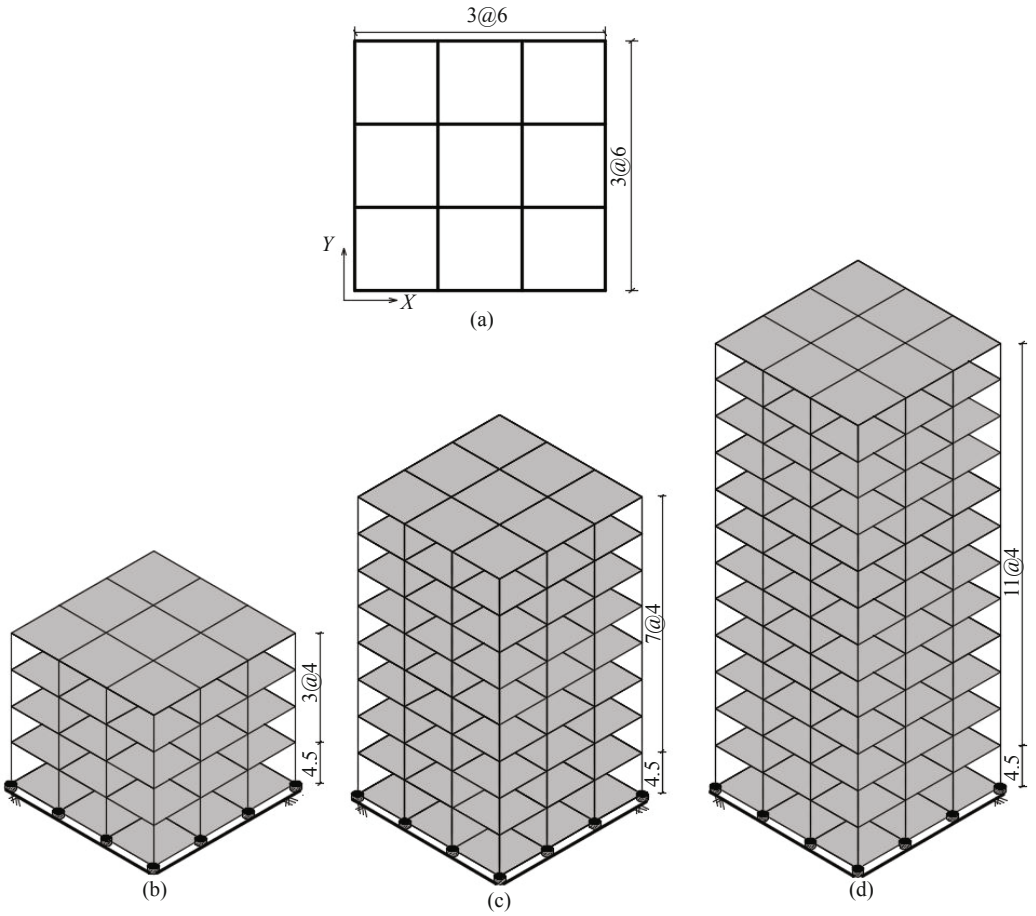

Fig. 1 Building configuration (all dimensions in m): (a) typical plan; (b) 4-story; (c) 8-story; (d) 12-story base-isolated buildings

Table 1 Beam size and reinforcement detailing

Building	Size (mm × mm)	Longitudinal reinforcement		Shear reinforcement[a]
		Top	Bottom	
4-story	625 × 550	6 No. 22	6 No. 19	4 legs at 120 mm
8-story	850 × 700	6 No. 32	6 No. 29	4 legs at 90 mm
12-story	1100 × 700	9 No. 36	9 No. 32	5 legs at 90 mm

[a]No. 10 bar was used as shear reinforcement

Table 2 Column size and reinforcement detailing

Building	Size (mm × mm)	Longitudinal reinforcement	Shear reinforcement[a]
4-story	625 × 625	16 No. 25	3 legs at 100 mm
8-story	850 × 850	20 No. 29	4 legs at 130 mm
12-story	1100 × 1100	24 No. 36	4 legs at 100 mm

[a]No. 10 bar was used as shear reinforcement

6.9 kN/m loads due to partitions and external cladding on the base beams and upper floor beams, respectively. Live load on the floor and roof slabs were taken as 4.8 kPa and 1.0 kPa, respectively. The total seismic weight of the 4-, 8-, and 12-story buildings was calculated to be 21,318 kN, 51,382 kN, and 91,002 kN, respectively.

The typical isolation system parameters considered in this study are normalized characteristic strength of the isolation system Q/W = 0.04 and 0.08 and isolation period T_{is} = 3.0 s, 3.5 s, and 4.0 s based on the post-elastic stiffness of the isolation system, where Q is the characteristic strength of isolation system and W is the total seismic weight of the building (Skinner *et al*., 1993; Naeim and Kelly, 1999). The superstructure is designed for the case when maximum forces get transmitted to the superstructure i.e., a combination of Q/W = 0.08 and T_{is} = 3.0 s The design of the 4-, 8-, and 12-story buildings was carried out to achieve similar performance in terms of base shear coefficient for the three buildings, and thereby to discuss the performance of the isolation

system. The response reduction factor is $R_I = 2$ for all the base-isolated buildings (Section 17.5.4.2, ASCE, 2010). It is noted that in real buildings located in high seismicity zones, RC shear wall frames would be used, at least for the 8- and 12-story buildings, instead of the special moment resisting frame systems adopted in this study. The fundamental periods of 4-, 8-, and 12-story buildings for a fixed-base condition are 0.63 s, 0.93 s, and 1.28 s, respectively.

A combination of lead rubber bearings (LRB) and natural rubber bearings (NRB) were used for the isolation system and the isolators were arranged symmetrically. A LRB and the corresponding force-deformation behavior is shown in Fig. 2. Both LB and UB values of the isolation system parameters, which incorporate the effect of aging of isolators (see Pavlou, 2005), have been taken into account and are listed in Table 3. The isolation system characteristics considering the UB model are shown in Table 4. The diameter of the bearings are 700 mm, 1000 mm, and 1200 mm for 4-, 8-, and 12-story buildings, respectively for both $Q/W = 0.04$ and 0.08. The diameter of lead core used for 4-, 8-, and 12-story buildings are 117 mm, 181 mm, and 242.5 mm, respectively for $Q/W = 0.04$; while 135 mm, 209 mm, and 278 mm are used for $Q/W = 0.08$. The rubber layers are 8 mm thick and the thickness of the steel shim is taken to be 2 mm. The shape factor of the isolators used in 4-, 8-, and 12-story buildings are calculated to be 21.875, 31.25, and 37.5, respectively. The cross-section of the NRB (which behaves in a linear elastic manner) is similar to the LRB but without the lead core.

3 Numerical modeling

Three-dimensional nonlinear finite element modeling was carried out using OpenSees (2013). Beams and columns were modeled using force-based, Euler-Bernoulli fiber beam-column elements with five integration points that account for the spread of inelasticity along the length of the element. A section discretized into unconfined concrete fibers, confined concrete fibers, and steel fibers was located at each integration point in the element. Uniaxial material models with a nonlinear constitutive relationship were assigned to the fibers. For concrete, Concrete02 material model was used, where the modified Kent and Park model (Park *et al.*, 1982) was used in compression, an initial linear elastic branch together with a linear softening branch up to zero stress was used in tension, and the model of Yassin (1994) was used to account for concrete damage and hysteresis. For reinforcing steel, Steel02 material model, which is based on the constitutive model of Menegotto and Pinto (1973), was used with a strain hardening ratio of 1%. Rigid diaphragms were used for the floors that enforce the rigid in-plane stiffness, whereas the out-of-plane stiffness was neglected. In this study, 1% stiffness-proportional damping was applied to the superstructure where the damping coefficient was calculated from the frequency of base-isolated building with the post-elastic stiffness of isolation system, based on the study of Pant *et al*. (2013b).

The lead rubber bearings with 10 mm yield displacement and natural rubber bearings used in this study were modeled using elastomeric bearing elements available in OpenSees. Calculated compressional and rotational stiffnesses were used for the isolators and 1% of the compressional stiffness was used to model the tension behavior of isolators in the vertical direction.

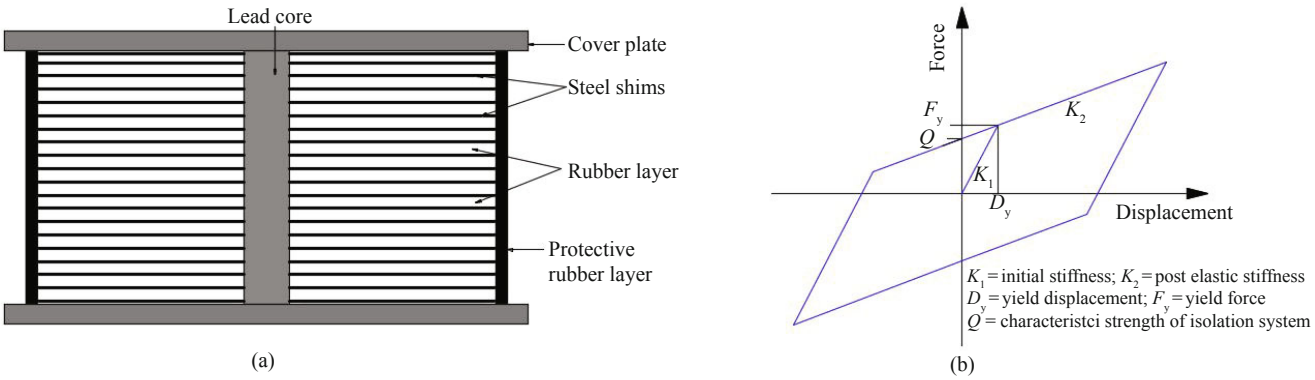

Fig. 2 (a) Typical configuration and (b) typical force-deformation relationship of lead rubber bearing

Table 3 Bounding values of the parameters for the isolation system (Pavlou, 2005)

	Lower bound	Upper bound
Shear modulus of rubber G (MPa)	0.45	0.55
Stiffening factor for lead f_L	0.95	1.05
Yield stress for lead σ_{YL}(MPa)	10	12

Table 4 Characteristics of the isolation systems considering UB properties of isolators

Building	Q/W	T_{is} (s)	DE			MCE_R		
			D_D (cm)	T_D (s)	β_D (%)	D_M (cm)	T_M (s)	β_M (%)
4-story	0.04	3.0	21.70	2.17	13.99	39.31	2.28	8.71
		3.5	22.66	2.43	17.23	42.56	2.62	10.65
		4.0	23.68	2.70	20.05	45.56	2.94	12.57
	0.08	3.0	13.80	1.75	28.77	26.70	2.02	20.02
		3.5	14.43	1.92	33.11	28.50	2.26	23.70
		4.0	14.68	2.04	36.84	29.76	2.46	27.21
8-story	0.04	3.0	21.71	2.17	14.00	39.34	2.28	8.64
		3.5	22.85	2.44	17.11	42.51	2.62	10.55
		4.0	23.80	2.70	19.87	45.80	2.94	12.44
	0.08	3.0	14.00	1.77	28.72	26.72	2.02	19.95
		3.5	14.44	1.92	32.94	28.52	2.26	23.47
		4.0	14.70	2.04	36.67	29.78	2.47	26.87
12-story	0.04	3.0	21.54	2.17	14.19	39.36	2.28	8.76
		3.5	22.65	2.43	17.32	42.47	2.62	10.67
		4.0	23.76	2.70	20.1	45.40	2.93	12.58
	0.08	3.0	14.03	1.77	28.72	26.75	2.03	19.97
		3.5	14.45	1.92	32.92	28.53	2.26	23.46
		4.0	14.77	2.04	36.61	29.80	2.47	26.87

T_{is} is the isolation period based on the post-elastic stiffness of the isolation system.
D_D, T_D and β_D are the displacement, effective period, and effective damping for the DE.
D_M, T_M and β_M are the displacement, effective period, and effective damping for the MCE_R.

4 Pushover analysis of the buildings

Pushover analysis of all the buildings under fixed-base condition considering P–Δ effects was carried out, using an inverted triangle load pattern. The pushover curves are shown in Fig. 3, where the base shear coefficient is defined as the ratio of base shear force to the total seismic weight of the building. The base shear capacity for the 4-, 8-, and 12-story buildings are 0.291W, 0.278W, and 0.275W, respectively, whereas the design base shear force is 0.154W for the superstructure of all the base-isolated buildings.

5 Earthquake ground motions

Two sets of ground motion were taken from Pacific Earthquake Engineering Research Center (PEER) database (PEER, 2013): the first set consists of 14 pairs of near-fault pulse type motions and the second set consists of 14 pairs of far-fault motions (Tables 5 and 6). Ground motions had been rotated to fault-normal (FN) and fault-parallel (FP) components. These ground motions were selected based on various criteria specified by FEMA P695 (FEMA, 2009) which are as follows: (i) magnitude of earthquake $M_w \geq 6.5$; (ii) closest distance

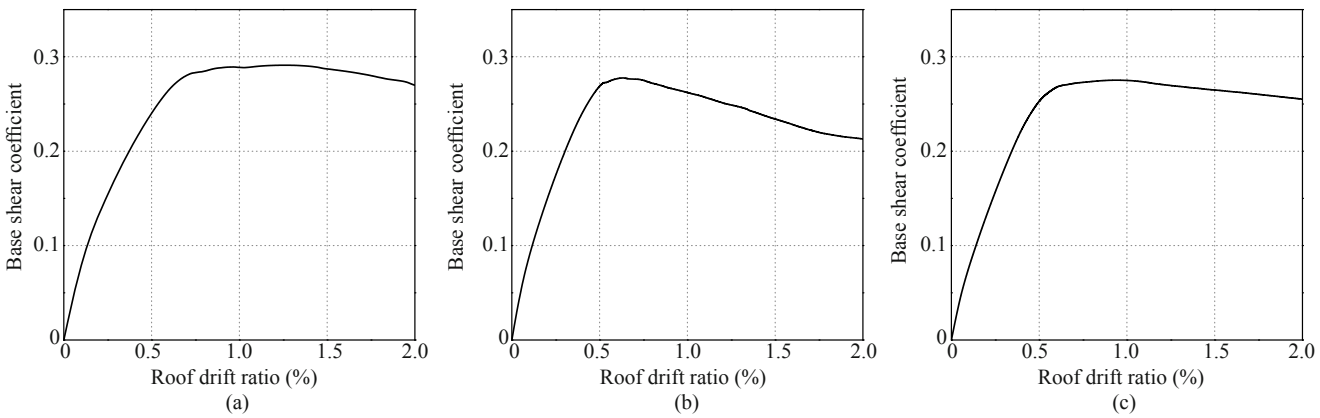

Fig. 3 Pushover curves in X-direction for the buildings: (a) 4-story; (b) 8-story; (c) 12-story

Table 5 Near-fault pulse-like ground motions scaled to represent MCE_R

GM No.	NGA seq. No.	Year	Event	Station	M_w	Scale factor	FN component		FP component	
							PGA (g)	T_p (s)	PGA (g)	T_p (s)
1	170	1979	Imperial Valley-06	EC County Center FF	6.5	1.45	0.26	4.5	0.32	-
2	179	1979	Imperial Valley-06	El Centro Array #4	6.5	1.09	0.39	4.6	0.52	-
3	182	1979	Imperial Valley-06	El Centro Array #7	6.5	0.92	0.42	4.2	0.31	4.5
4	184	1979	Imperial Valley-06	El Centro Differential Array	6.5	1.45	0.60	5.9	0.64	2.0
5	802	1989	Loma Prieta	Saratoga-Aloha Ave	6.9	1.70	0.62	4.5	0.64	-
6	803	1989	Loma Prieta	Saratoga-W Valley Coll.	6.9	1.32	0.53	1.9	0.34	5.0
7	821	1992	Erzican, Turkey	Erzincan	6.7	0.94	0.46	2.7	0.39	2.2
8	1013	1994	Northridge-01	LA Dam	6.7	1.15	0.66	1.7	0.48	2.8
9	1176	1999	Kocaeli, Turkey	Yarimca	7.5	0.86	0.24	-	0.27	4.6
10	1510	1999	Chi-Chi, Chinese Taipei	TCU075	7.6	1.07	0.36	5.0	0.29	-
11	1511	1999	Chi-Chi, Chinese Taipei	TCU076	7.6	1.32	0.40	4.0	0.55	-
12	1515	1999	Chi-Chi, Chinese Taipei	TCU082	7.6	1.57	0.39	9.2	0.31	-
13	1605	1999	Duzce, Turkey	Duzce	7.1	1.01	0.36	-	0.52	5.6
14	2114	2002	Denali, Alaska	TAPS Pump Station #10	7.9	0.79	0.26	-	0.22	5.7

NGA seq. No.: Next generation attenuation project database sequence number.
FN: fault-normal; FP: fault-parallel.
PGA: Peak ground acceleration.
T_p: Velocity pulse period.

Table 6 Far-fault ground motions scaled to represent MCE_R

GM No.	NGA seq. No.	Year	Event	Station	M_w	Scale factor	FN component	FP component
							PGA (g)	PGA (g)
1	139	1978	Tabas, Iran	Dayhook	7.4	2.76	0.84	0.99
2	169	1979	Imperial Valley	Delta	6.5	1.78	0.43	0.57
3	175	1979	Imperial Valley	Array #12	6.5	3.43	0.39	0.48
4	728	1987	Superstition Hills	Westmorland Fire Sta.	6.5	1.90	0.40	0.45
5	729	1987	Superstition Hills	Wildlife Liquef. Array	6.5	1.45	0.30	0.27
6	776	1989	Loma Prieta	Hollister-South & Pine	6.9	1.18	0.32	0.35
7	778	1989	Loma Prieta	Hollister DA	6.9	1.73	0.48	0.50
8	832	1992	Landers	Amboy	7.3	2.81	0.41	0.31
9	888	1992	Landers	San Bernardino	7.3	2.62	0.21	0.23
10	1113	1995	Kobe, Japan	OSAJ	6.9	3.17	0.23	0.26
11	1155	1999	Kocaeli, Turkey	Bursa Tofas	7.5	2.89	0.30	0.31
12	1187	1999	Chi-Chi, Chinese Taipei	CHY015	7.6	2.06	0.34	0.36
13	1208	1999	Chi-Chi, Chinese Taipei	CHY046	7.6	2.62	0.36	0.42
14	1810	1999	Hector Mine	Mecca	7.1	3.67	0.35	0.45

NGA seq. No.: Next generation attenuation project database sequence number.
FN: fault-normal; FP: fault-parallel.
PGA: Peak ground acceleration.

to fault rupture $R_{rup} \leq 10$ km for the near-fault set and $10 < R_{rup} \leq 100$ km for the far-fault set; (iii) lowest usable frequency of ground motions less than 0.167 Hz; and (iv) site class for recording station is either C or D. Selected ground motions were scaled to match the MCE_R-level target acceleration spectrum using the weighted scale method for a period range of 1.01 to 4.40 s (Fig. 4) which includes the recommended range by ASCE 7-10 (ASCE, 2010) of $0.5T_D$ to $1.25T_M$ for base-isolated buildings. Here, $T_D = 2.02$ s (shortest T_D) and $T_M = 3.50$ s (longest T_M) are the effective periods of the isolation system at the design and maximum displacements, respectively (Table 4). The acceleration time histories of records scaled to represent the MCE_R-level are multiplied by 2/3 to obtain the records for DE-level.

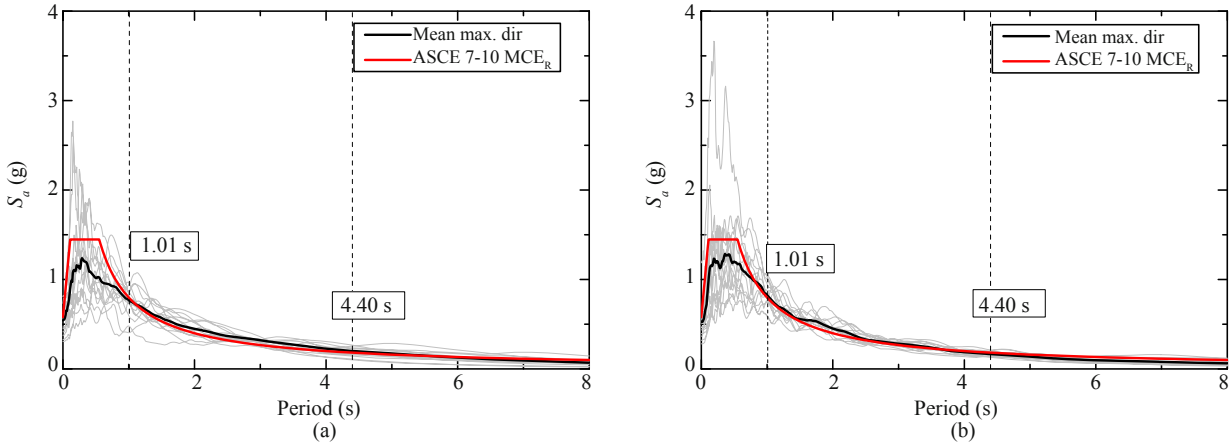

Fig. 4 Comparison of 5%-damped mean acceleration response spectrum of scaled ground motions with the MCE$_R$-level code spectrum: (a) near-fault; (b) far-fault

6 Results of nonlinear response history analysis

Nonlinear response history analyses of the buildings were carried out for LB and UB properties of the isolation system under DE-level and MCE$_R$-level for both sets of ground motions. The numerical models of the buildings with LB and UB properties of isolators are hereafter referred to as LB model and UB model, respectively. In the present study, FN and FP components of ground motion were taken to correspond to *X*-direction and *Y*-direction, respectively (see Fig. 1(a)). First, the peak response indicators for the buildings with different isolation system parameters are presented. Next, the responses of the base-isolated buildings are compared with those of the fixed-base buildings. Finally, the applicability of a rigid superstructure assumption to predict the isolation system displacement demand is discussed.

6.1 Superstructure response of 4-, 8-, and 12-story base-isolated buildings under DE-level and MCE$_R$-level ground motions

The superstructure response is discussed in terms of mean values of peak inter-story drift ratio, peak normalized story shear force, and peak absolute floor acceleration. The story shear force was normalized by the total seismic weight W of the buildings. Since the mean values of the *X*-direction response indicators were found to be larger than in the *Y*-direction, inter-story drift ratio and normalized story shear force are shown only for the *X*-direction. Floor accelerations are presented as the resultant of the demands in two orthogonal directions. Peak inter-story drift ratios in the ranges of 0.2%–0.5%, 0.5%–1.5%, and 1.5%–3% correspond to damage of drift-sensitive nonstructural components, moderate structural damage, and severe structural damage, respectively (Elnashai and Di Sarno, 2008). A peak inter-story drift ratio greater than 3% can be assumed to correspond to a collapsed story. Since the superstructure response is greater for the UB model as larger forces are transmitted to the superstructure, only results with the UB model are presented.

The peak inter-story drift ratios (IDR) under DE-level and MCE$_R$-level near-fault motions are shown in Fig. 5. The peak IDRs of all the buildings are less than 0.5% under DE-level ground motions (Figs. 5(a)-(c)), indicating that there is no structural damage; but under MCE$_R$-level ground motions there is moderate structural damage to the buildings as the maximum value of peak IDR exceeds 0.5% but is well below 1.5% (Figs. 5(d)-(f)). Under both levels of ground motion, the peak IDR is largest at the first floor level for 4-story buildings but for 8-story and 12-story buildings, it increases and then decreases with the floor level. This could be due to the influence of higher modes as the height of the building increases. The peak IDRs are generally larger for Q/W = 0.08 compared to Q/W = 0.04 under DE-level ground motions, whereas the peak IDR are larger for Q/W = 0.04 under MCE$_R$-level ground motions.

Far-fault motions result in smaller values of the peak IDR compared to near-fault motions (Fig. 6). Under DE-level and MCE$_R$-level ground motions, the peak IDR is below 0.5% at all floor levels indicating that the buildings sustain no structural damage; however, structural damage is indicated for the case of MCE$_R$-level near-fault motions. The trend of the peak IDR along the height of the buildings is similar under near-fault and far-fault motions.

Since, the smallest isolation period T_{is} results in maximum superstructure response, for conciseness, a comparison of maximum values of IDR for near-fault and far-fault motions under DE-level and MCE$_R$-level for T_{is} = 3.0 s is done (Fig. 7). Under DE-level ground motions, there is no significant difference in the IDR between Q/W = 0.04 and Q/W = 0.08 for both near-fault and far-fault motions (Fig. 7(a)). However, near-fault motions resulted up to 28% (33%) larger IDR for

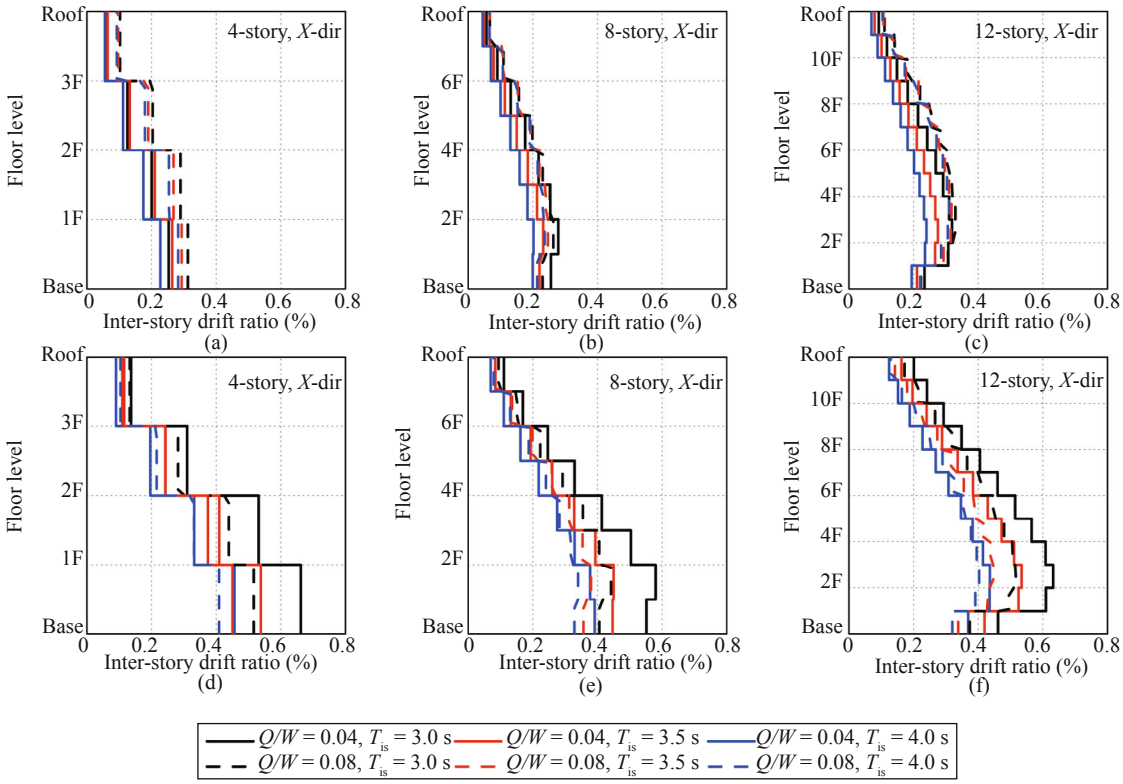

Fig. 5 Mean values of peak inter-story drift ratio for 4-, 8-, and 12-story buildings with UB properties of isolators under near-fault motions: (a)–(c) DE-level; (d)–(f) MCE_R-level

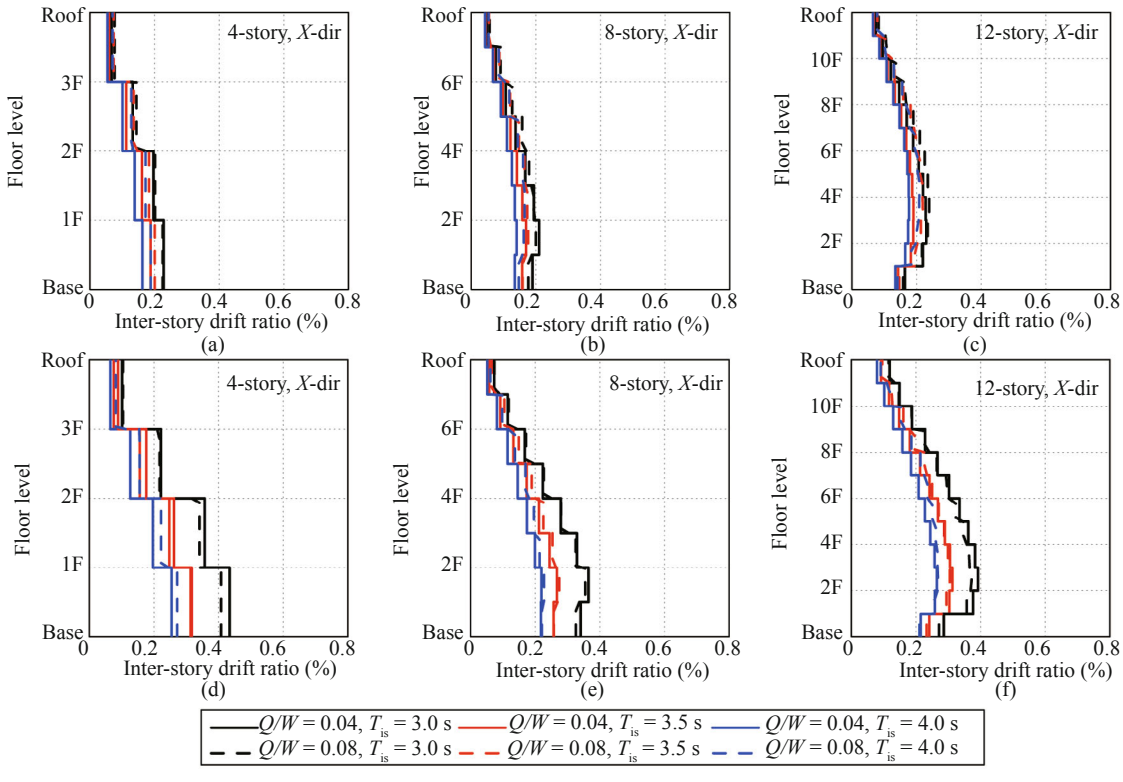

Fig. 6 Mean values of peak inter-story drift ratio for 4-, 8-, and 12-story buildings with UB properties of isolators under far-fault motions: (a)–(c) DE-level; (d)–(f) MCE_R-level

$Q/W = 0.04$ ($Q/W = 0.08$) compared to far-fault motions. Under MCE_R-level far-fault motions, for $Q/W = 0.04$ and $Q/W = 0.08$, the IDR is nearly the same (Fig. 7(b)), but significant difference can be observed for the case of

near-fault motions. Compared to far-fault motions, near-fault motions results in larger IDR up to 29% for Q/W = 0.04 and 38% for Q/W = 0.08.

The peak normalized story shear forces under DE-level and MCE_R-level near-fault motions are shown in Fig. 8. The peak normalized story shear force has the same trend for all the buildings under DE-level and MCE_R-level ground motions. The maximum base shear force under DE-level ground motions is about 0.15W (Figs. 8(a)-(c)) which is almost equal to the design base shear force. The base shear demand is well below the base shear capacity (see Fig. 3) for all the buildings even under MCE_R-level ground motions (Figs. 8(d)-(f)). The story shear force is greater for Q/W = 0.08 under DE-level ground motions for all the buildings, but Q/W = 0.04 generally results in larger story shear force demand under MCE_R-level ground motions.

Far-fault motions result in smaller peak normalized story shear force compared to near-fault motions under DE and MCE_R-levels (Fig. 9). The trend of the normalized story shear force along the height is the same for all the building as is with the case of near-fault motions.

The results for the peak floor accelerations under DE-level and MCE_R-level near-fault motions are shown in Fig. 10. Under DE-level near-fault motions, the peak

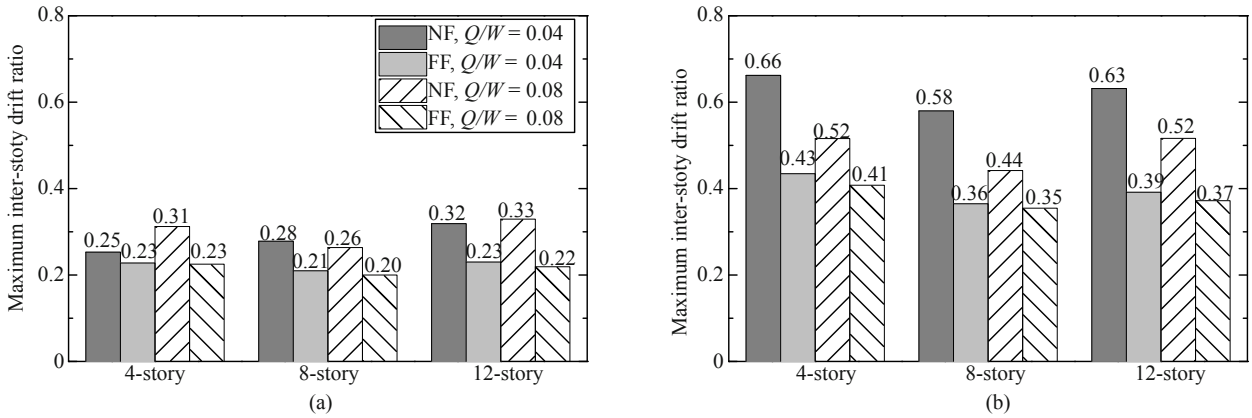

Fig. 7 Comparison of maximum inter-story drift ratio between near-fault and far-fault motions for isolation period of T_{is} = 3.0 s: (a) DE-level; (b) MCE_R-level. Here, NF represents near-fault and FF represents far-fault motions

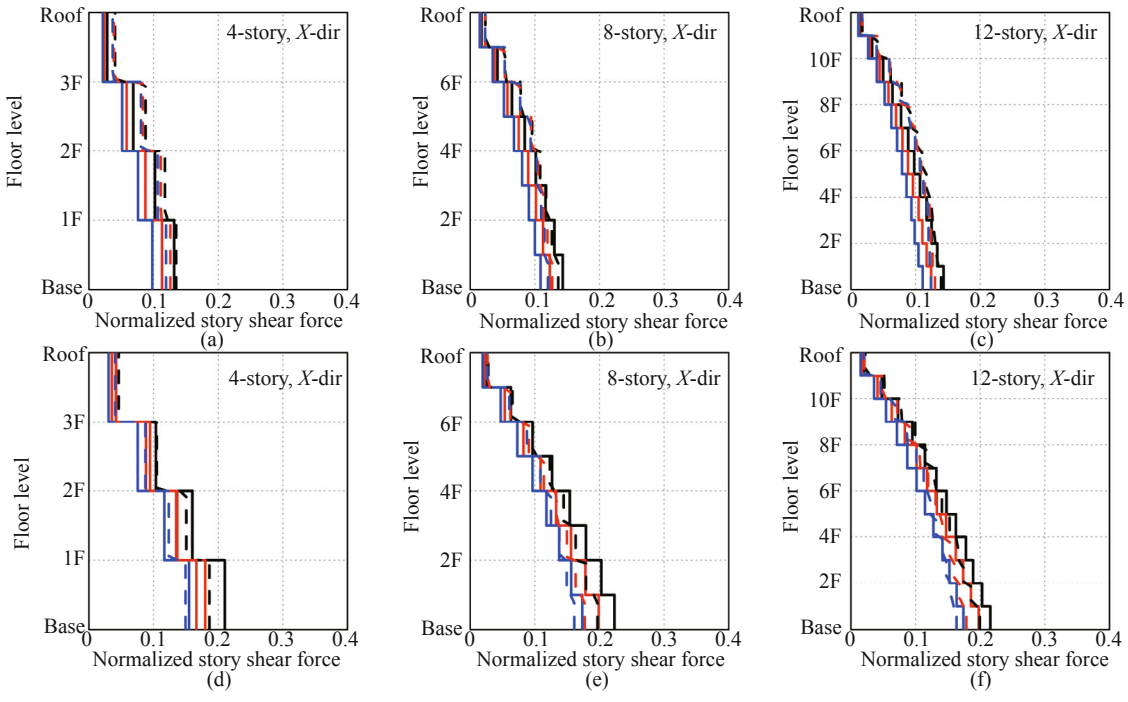

Fig. 8 Mean values of peak normalized story shear force for 4-, 8-, and 12-story buildings with UB properties of isolators under near-fault motions: (a)–(c) DE-level; (d)–(f) MCE_R-level

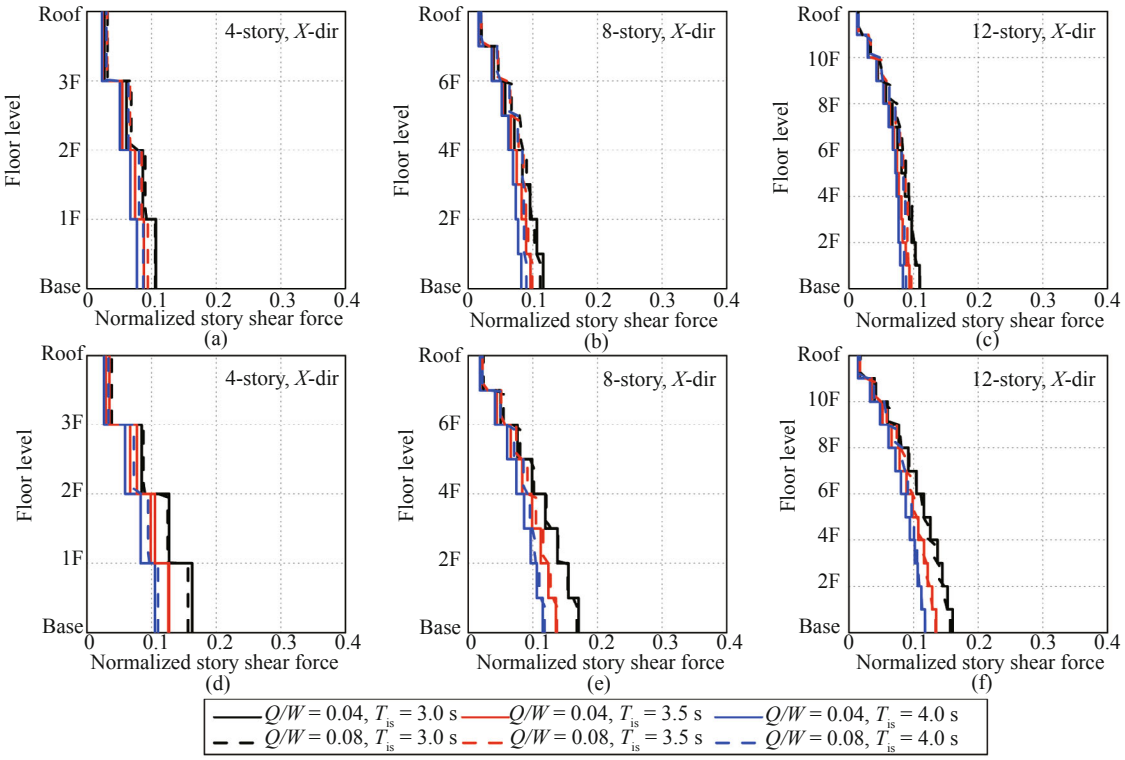

Fig. 9 Mean values of peak normalized story shear force for 4-, 8-, and 12-story buildings with UB properties of isolators under far-fault motions: (a)–(c) DE-level; (d)–(f) MCE_R-level

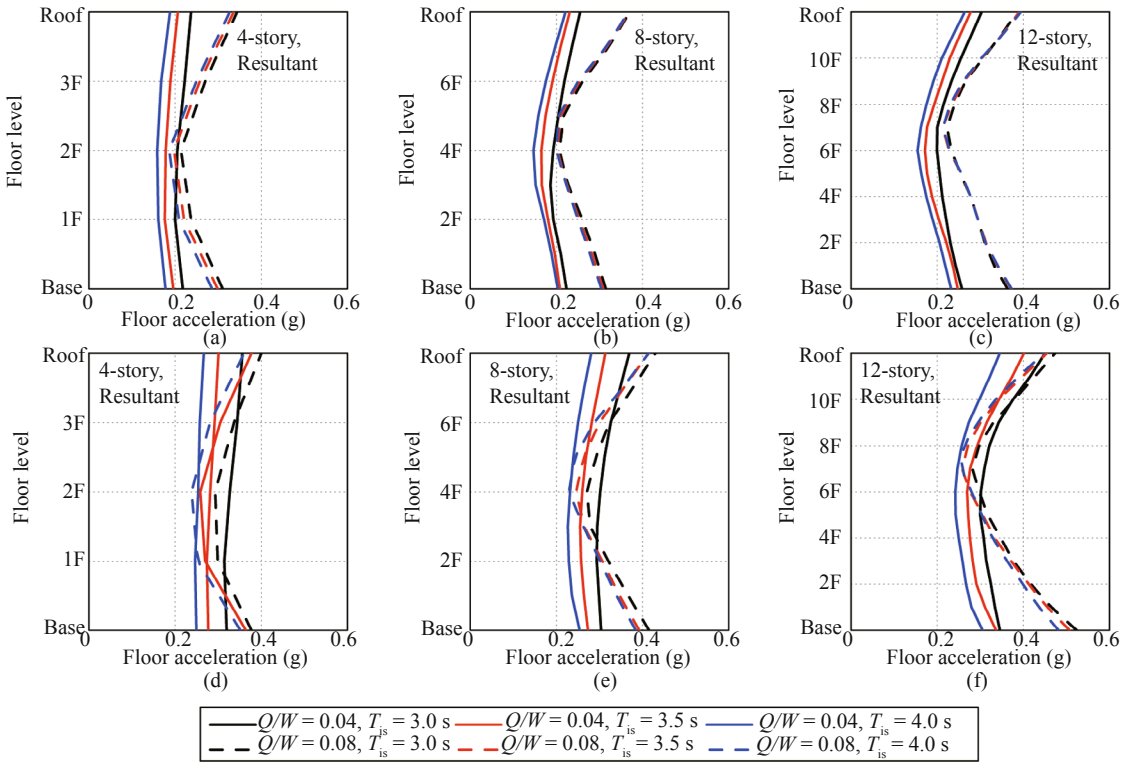

Fig. 10 Mean values of peak floor acceleration for 4-, 8-, and 12-story buildings with UB properties of isolators under near-fault motions: (a)–(c) DE-level; (d)–(f) MCE_R-level

floor accelerations at the base and roof levels for all the buildings when Q/W = 0.08 are greater than 0.3 g (Figs. 10(a)-(c)), which is often referred to as a limit in the design of seismically isolated buildings (Pan *et al.*, 2005), whereas it is below this limit for Q/W = 0.04. At the lower floor levels and upper floor levels, under

MCE_R-level ground motions, the peak floor accelerations are larger for Q/W = 0.08 when compared with Q/W = 0.04 and greater than 0.3 g (Figs. 10(d)-(f)). When the number of stories in a building increases, the peak floor accelerations are seen to increase under both levels of ground motion.

Compared to near-fault motions, the results of the peak floor accelerations are smaller under far-fault motions (Fig. 11). The peak floor accelerations are less than 0.3 g for Q/W = 0.04 while they are slightly greater than 0.3 g for 8- and 12-story buildings when Q/W = 0.08 under DE-level ground motions. Under MCE_R-level ground motions, the peak floor accelerations exceed 0.3 g at some of the lower floor levels and upper floor levels for both the values of Q/W. A smaller isolation period T_{is} and a larger value of normalized characteristic strength of the isolation system Q/W result in larger peak accelerations at the base and roof levels; this trend is similar to that for near-fault motions.

In Fig. 12 the peak roof accelerations for near-fault and far-fault motions are compared for isolation period T_{is} = 3.0 s. It is seen that the peak roof accelerations for near-fault and far-fault motions result in nearly the same values for Q/W = 0.04, while a variation up to 16% is seen for Q/W = 0.08 under DE-level ground motions (Fig. 12(a)). However, MCE_R-level near-fault motions result in larger peak roof acceleration up to 11% for Q/W = 0.04 and 17% for Q/W = 0.08 (Fig. 12(b)).

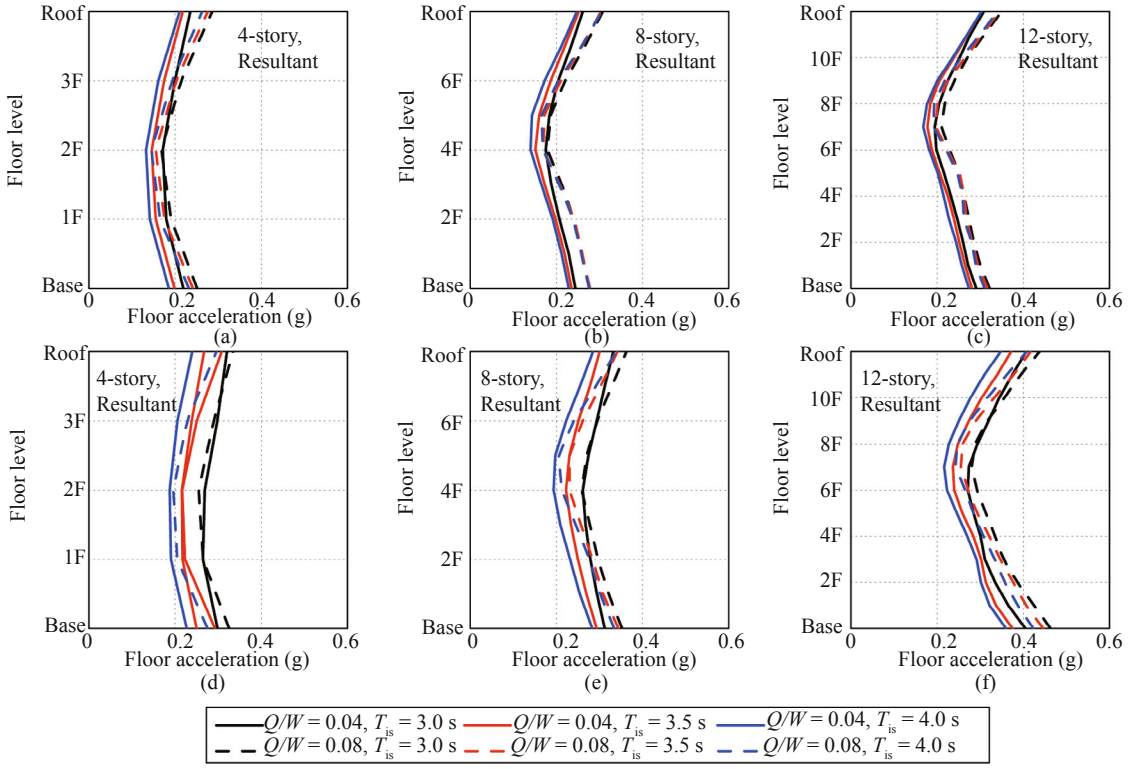

Fig. 11 Mean values of peak floor acceleration for 4-, 8-, and 12-story buildings with UB properties of isolators under far-fault motions: (a)–(c) DE-level; (d)–(f) MCE_R-level

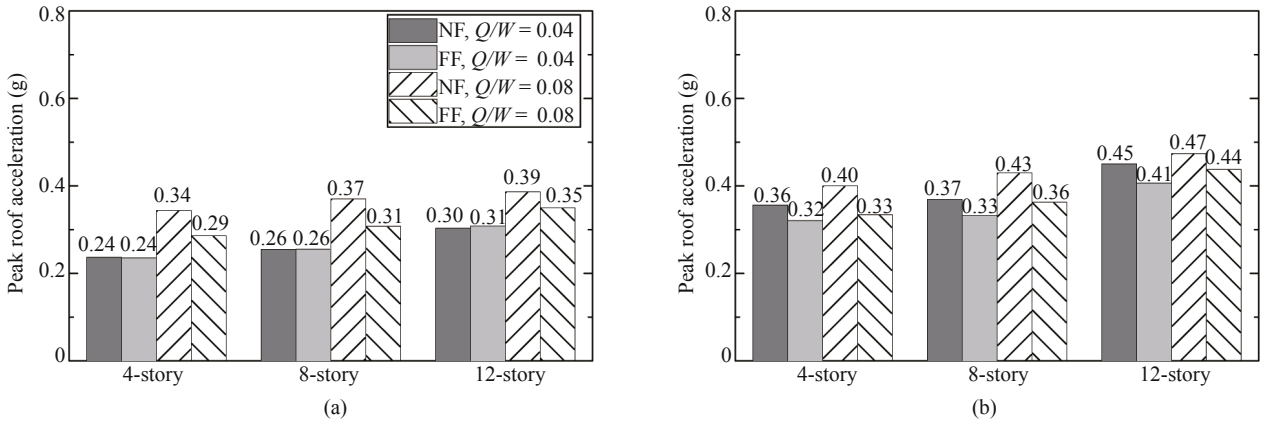

Fig. 12 Comparison of peak roof acceleration between near-fault and far-fault motions for isolation period of T_{is} = 3.0 s: (a) DE-level; (b) MCE_R-level. Here, NF represents near-fault and FF represents far-fault motions

6.2 Superstructure response of 4-, 8-, and 12-story buildings with a fixed-base condition under DE-level and MCE_R-level ground motions

The performance of the buildings in a fixed-base condition is investigated in order to evaluate the response reduction of the superstructure by the use of isolation systems. The results for the fixed-base buildings for near-fault and far-fault motions are shown in Figs. 13 and 14, respectively. When the response of the base-isolated buildings plotted in Figs. 5, 6, 8-11 are compared with the response of the fixed-base buildings plotted in Figs. 13 and 14, it is seen that the use of base isolation leads to a significant reduction of the superstructure response. The peak inter-story drift ratio and peak normalized story shear force (the maximum of all floor levels), and the peak roof acceleration of the fixed base buildings are compared with the base-isolated building response in Tables 7 and 8. The fixed-base buildings developed significant inelastic deformation at the MCE_R-level as the maximum value of peak inter-story drift ratio along all floor levels reached 1.62%, 1.46%, and 1.19% (1.36%, 1.19%, and 1.02%) for 4-, 8-, and 12-story buildings under near-fault (far-fault) motions. These values are significantly larger compared to base-isolated buildings where the peak inter-story drift ratio were 0.46%, 0.39%, and 0.44% (0.25%, 0.22%, and 0.26%) for 4-, 8-, and 12-story buildings under near-fault (far-fault) motions. The peak normalized story shear force at the base level for the fixed-base buildings are larger than the design base shear of $0.154W$ under DE-level and MCE_R-level near-fault and far-fault motions. With the use of an isolation system, the peak normalized story shear force in the 4-story building is reduced from 0.27 (0.27) to 0.15 (0.11) under MCE_R-level near-fault (far-fault) motions. Similar reductions can also be observed

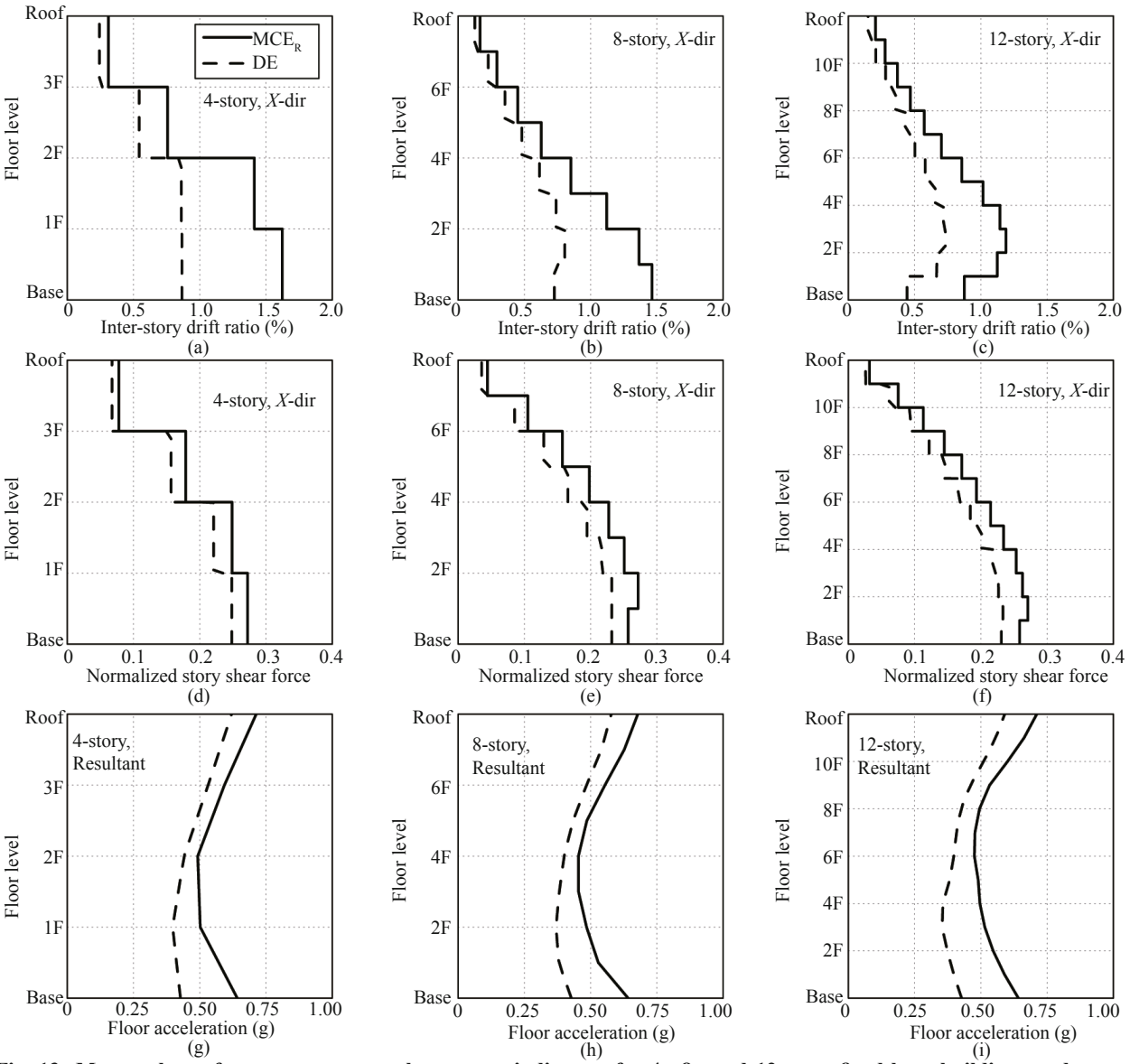

Fig. 13 Mean values of superstructure peak response indicators for 4-, 8-, and 12-story fixed-base buildings under near-fault motions: (a)–(c) inter-story drift ratio; (d)–(f) normalized story shear force; (g)–(i) floor acceleration

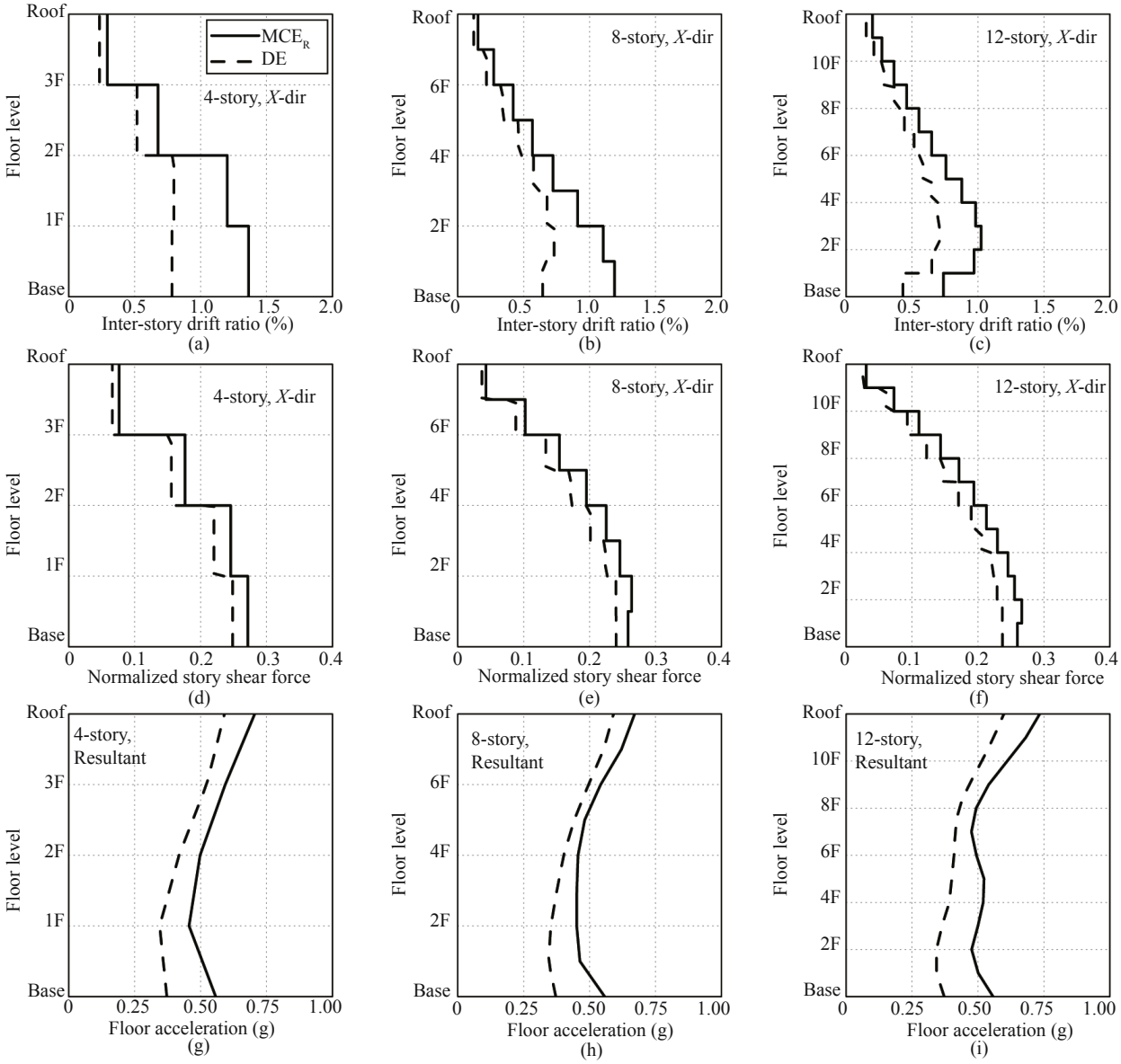

Fig. 14 Mean values of superstructure peak response indicators for 4-, 8-, and 12-story fixed-base buildings under far-fault motions: (a)–(c) inter-story drift ratio; (d)–(f) normalized story shear force; (g)–(i) floor acceleration

Table 7 Comparison of superstructure peak response of fixed-base and base-isolated buildings under near-fault ground motions

Building	Inter-story drift ratio[1] (%)				Normalized story shear force[1]				Roof acceleration[2] (g)			
	Fixed-base		Base-isolated		Fixed-base		Base-isolated		Fixed-base		Base-isolated	
	DE	MCE$_R$	DE	MCE$_R$	DE	MCE$_R$	DE	MCE$_R$	DE	MCE$_R$	DE	MCE$_R$
4-story	0.86	1.62	0.23	0.46	0.25	0.27	0.10	0.15	0.62	0.71	0.19	0.27
8-story	0.80	1.46	0.20	0.39	0.23	0.27	0.09	0.17	0.58	0.68	0.22	0.28
12-story	0.73	1.19	0.24	0.44	0.23	0.27	0.11	0.17	0.59	0.71	0.26	0.35

[1]Inter-story drift ratio and Normalized story shear force:
Fixed-base building - maximum of all floor levels.
Base-isolated building - minimum value at corresponding floor level considering all base-isolated buildings.
[2]Roof acceleration: Base-isolated building - minimum value considering all base-isolated buildings.

for 8- and 12-story buildings. Peak roof accelerations are also found to be reduced significantly in base-isolated buildings compared to fixed-base buildings. Peak roof accelerations reduce from 0.71 g (0.71 g) to 0.27 g (0.24 g) in 4-story buildings with the use of isolation system under MCE$_R$-level near-fault (far-fault) motions. A similar trend is also seen for the 8- and 12-story buildings. Observing the overall performance of the

Table 8 Comparison of superstructure peak response of fixed-base and base-isolated buildings under far-fault ground motions

Building	Inter-story drift ratio[1] (%)				Normalized story shear force[1]				Roof acceleration[2] (g)			
	Fixed-base		Base-isolated		Fixed-base		Base-isolated		Fixed-base		Base-isolated	
	DE	MCE_R	DE	MCE_R	DE	MCE_R	DE	MCE_R	DE	MCE_R	DE	MCE_R
4-story	0.80	1.36	0.16	0.25	0.25	0.27	0.08	0.11	0.59	0.71	0.21	0.24
8-story	0.73	1.19	0.14	0.22	0.24	0.26	0.08	0.12	0.59	0.67	0.25	0.29
12-story	0.71	1.02	0.17	0.26	0.24	0.26	0.08	0.12	0.60	0.73	0.30	0.35

[1]Inter-story drift ratio and Normalized story shear force:
Fixed-base building - maximum of all floor levels.
Base-isolated building - minimum value at corresponding floor level considering all base-isolated buildings.
[2]Roof acceleration: Base-isolated building - minimum value considering all base-isolated buildings.

buildings in fixed-base and base-isolated conditions, the superstructure response is found to be significantly reduced in base-isolated buildings.

To investigate the behavior of columns that have yielded, the axial force-biaxial moment response corresponding to maximum axial force P, maximum M_X, and maximum M_Y for a 1st floor column of the 4-story building under MCE_R-level near-fault motion of Erzican, Turkey earthquake is shown in Fig. 15. The section has yielded as seen in Fig. 15(c).

6.3 Comparison of isolation system displacement when buildings are modeled with a rigid superstructure and a flexible superstructure

When the superstructure is assumed to be rigid, the entire superstructure is modeled as a SDF system where the total mass of the superstructure is lumped on top of the bearing. The mean values of peak relative base displacement for base-isolated buildings modeled with a rigid superstructure and a flexible superstructure under near-fault motions are shown in Fig. 16. Since the isolation system displacement is governed by LB properties of isolators, for brevity, results using only the LB model are presented. Also plotted in Fig. 16 is a solid line with slope equal to one for reference. Any point lying below the solid line indicates that consideration of a rigid superstructure provides a conservative estimate of base displacements. The displacements are presented as the resultant of the displacement response in two orthogonal directions.

Figure 16 shows that the mean values of peak relative base displacement under near-fault motions are well estimated when the superstructure is modeled as a rigid body. As expected, when the normalized characteristic strength of the isolation system Q/W increases, there is a decrease in peak base displacement. Under DE-level ground motions (Figs. 16(a)–(c)), consideration of a rigid superstructure assumption underestimated the peak base displacements at most by 1.5% for the 12-story buildings. For the 4- and 8-story buildings under DE-level ground motions, the peak base displacements are found to be well estimated with a maximum overestimation of 6% for the 8-story buildings. Under MCE_R-level ground motions (Figs. 16(d)–(f)), for a building with the same number of stories and Q/W = 0.04, a significant

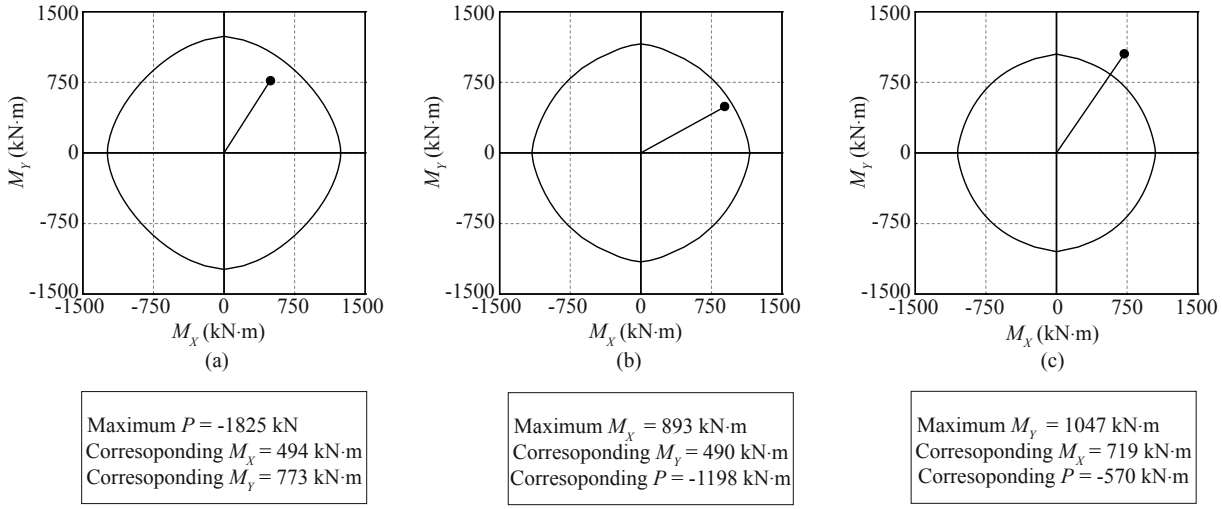

Fig. 15 Axial force-biaxial moment response for a 1st floor column of the 4-story building under MCE_R-level near-fault motion of Erzican, Turkey earthquake: (a) for maximum axial force P; (b) for maximum M_X; (c) for maximum M_Y

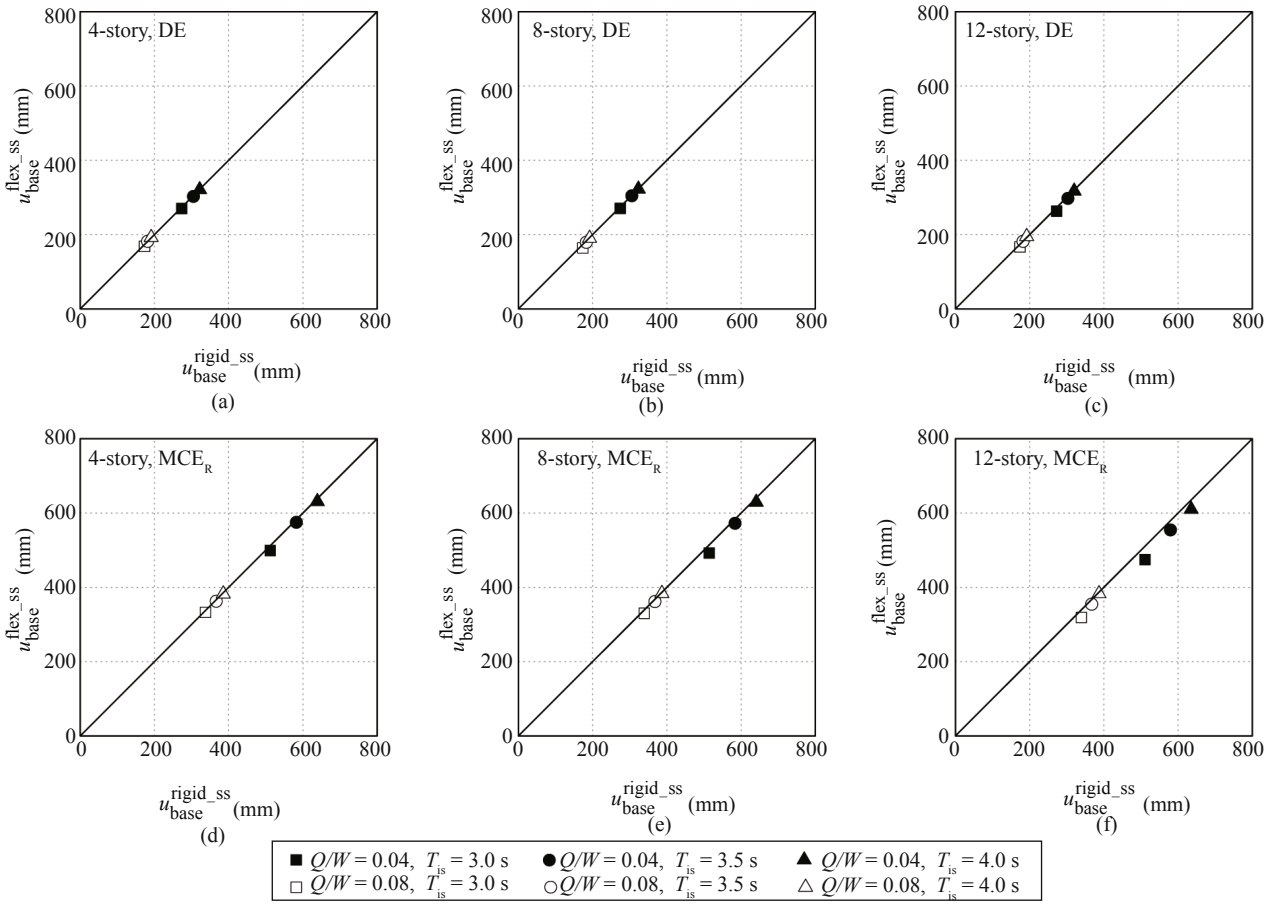

Fig. 16 Comparison of mean values of peak relative base displacement for buildings with superstructure modeled as rigid ($u_{base}^{rigid\_ss}$) and superstructure modeled as flexible ($u_{base}^{flex\_ss}$) for 4-, 8-, and 12-story buildings with LB properties of isolators under near-fault motions: (a)–(c) DE-level; (d)–(f) MCE$_R$-level. A solid line with slope equal to one is shown for reference

increase in peak base displacement is observed when the isolation period T_{is} increases, which is not seen under DE-level ground motions. Under MCE$_R$-level ground motions, when a rigid superstructure is assumed, peak base displacements are at most overestimated by 8% for the 12-story buildings. This suggests that a rigid superstructure assumption may be sufficient to obtain the peak base displacement for a base-isolated building with an elastomeric bearing isolation system, since higher modes of a superstructure do not contribute significantly to the bearing displacements.

7 Conclusions

In the present study, the response of 4-, 8-, and 12-story base-isolated buildings under bidirectional near-fault pulse-like motions and far-fault motions scaled to represent DE and MCE$_R$, was investigated. Both LB and UB properties of the isolation system were considered. The major conclusions drawn from this study are as follows:

(1) The peak inter-story drift ratios under DE-level motions and MCE$_R$-level far-fault motions correspond to no structural damage, whereas minor structural damage is indicated under MCE$_R$-level near-fault motions.

(2) The base shear demands in the superstructure are well below their corresponding capacities for near-fault motions under MCE$_R$-level.

(3) The peak floor accelerations are larger for the higher Q/W value (i.e., Q/W = 0.08) for near-fault and far-fault motions under both DE and MCE$_R$-levels at lower floor levels and upper floor levels and are found to increase with the increase in number of stories. Under MCE$_R$-level near-fault and far-fault motions the peak floor accelerations exceed 0.3 g at some of the lower floor levels and upper floor levels for both values of Q/W, while 0.3 g is exceeded only for Q/W = 0.08 under DE-level motions.

(4) Base isolation significantly improves the superstructure performance when compared to a fixed-base condition even for a flexible 12-story building.

(5) Peak relative base displacements obtained by modeling the superstructure either as rigid or as flexible are found to be nearly the same in all the buildings, for the range of isolation system parameters considered. Thus, the rigid superstructure assumption provides a proper estimate of peak base displacement in the case of base-isolated buildings up to 12-stories.

References

ACI (2011), *Building Code Requirements for Structural Concrete* (*ACI 318-11*), American Concrete Institute (ACI), Farmington Hills, MI, USA.

Alhan C and Gavin H (2004), "A Parametric Study of Linear and Non-linear Passively Damped Seismic Isolation Systems for Buildings," *Engineering Structures*, **26**(4): 485–497.

Alhan C and Sürmeli M (2011), "Shear Building Representations of Seismically Isolated Buildings," *Bulletin of Earthquake Engineering*, **9**(5): 1643–1671.

Ariga T, Kanno Y and Takewaki I (2006), "Resonant Behaviour of Base-isolated High-rise Buildings Under Long-period Ground Motions," *The Structural Design of Tall and Special Buildings*, **15**(3): 325–338.

ASCE (2010), *Minimum Design Loads for Buildings and Other Structures* (*ASCE 7-10*), American Society of Civil Engineers (ASCE), Reston, VA, USA.

Becker TC and Mahin SA (2013), "Approximating Peak Responses in Seismically Isolated Buildings Using Generalized Modal Analysis," *Earthquake Engineering and Structural Dynamics*, **42**(12): 1807–1825.

Calugaru V and Panagiotou M (2014), "Seismic Response of 20-story Base-isolated and Fixed-base Reinforced Concrete Structural Wall Buildings at a Near-fault Site," *Earthquake Engineering and Structural Dynamics*, **43**(6): 927–948.

Castaldo P, Palazzo B and Della Vecchia P (2015), "Seismic Reliability of Base-isolated Structures with Friction Pendulum Bearings," *Engineering Structures*, **95**: 80–93.

Chimamphant S and Kasai K (2016), "Comparative Response and Performance of Base-isolated and Fixed-base Structures," *Earthquake Engineering and Structural Dynamics*, **45**(1): 5–27.

Di Sarno L, Chioccarelli and Cosenza E (2011), "Seismic Response Analysis of an Irregular Base-isolated Building," *Bulletin of Earthquake Engineering*, **9**(5): 1673–1702.

Elnashai AS and Di Sarno L (2008), *Fundamentals of Earthquake Engineering*, Wiley, United Kingdom.

Fadi F and Constantinou MC (2010), "Evaluation of Simplified Methods of Analysis for Structures with Triple Friction Pendulum Isolators," *Earthquake Engineering and Structural Dynamics*, **39**(1): 5–22.

FEMA (2009), *Quantification of Building Seismic Performance Factors (FEMA P695)*, Federal Emergency Management Agency (FEMA), Washington, DC, USA.

Hall JF, Heaton TH, Halling MW and Wald DJ (1995), "Near-source Ground Motion and Its Effects on Flexible Buildings," *Earthquake Spectra*, **11**(4): 569–605.

ICC (2012), *International Building Code*, International Code Council (ICC), Country Club Hills, IL, USA.

Jangid RS and Kelly JM (2000), "Torsional Displacements in Base-isolated Buildings," *Earthquake Spectra*, **16**(2): 443–454.

Jangid RS and Kelly JM (2001), "Base Isolation for Near-fault Motions," *Earthquake Engineering and Structural Dynamics*, **30**(5): 691–707.

Kalpakidis IV, Constantinou MC and Whittaker AS (2010), "Modeling Strength Degradation in Lead–rubber Bearings Under Earthquake Shaking," *Earthquake Engineering and Structural Dynamics*, **39**(13): 1533–1549.

Kilar V and Koren D (2009), "Seismic Behaviour of Asymmetric Base-isolated Structures with Various Distributions of Isolators," *Engineering Structures*, **31**(4): 910–921.

Mahmoud S, Austrell PE and Jankowski R (2012), "Simulation of the Response of Base-isolated Buildings under Earthquake Excitations Considering Soil Flexibility," *Earthquake Engineering and Engineering Vibration*, **11**(3): 359–374.

Mahmoud S and Gutub S (2013), "Earthquake Induced Pounding-involved Response of Base-isolated Buildings Incorporating Soil Flexibility," *Advances in Structural Engineering*, **16**(12): 2043–2062.

Masroor A and Mosqueda G (2015), "Assessing the Collapse Probability of Base-isolated Buildings Considering Pounding to Moat Walls Using the FEMA P695 Methodology," *Earthquake Spectra*, **31**(4): 2069–2086.

Matsagar VA and Jangid RS (2004), "Influence of Isolator Characteristics on the Response of Base-isolated Structures," *Engineering Structures*, **26**(12): 1735–1749.

Mazza F and Vulcano A (2009), "Nonlinear Response of RC Framed Buildings with Isolation and Supplemental Damping at the Base Subjected to Near-fault Earthquakes," *Journal of Earthquake Engineering*, **13**(5): 690–715.

Mazza F and Vulcano A (2012), "Effects of Near-fault Ground Motions on the Nonlinear Dynamic Response of Base-isolated R.C. Framed Buildings," *Earthquake Engineering and Structural Dynamics*, **41**(2): 211-232.

Menegotto M and Pinto P (1973), "Methods of Analysis for Cyclically Loaded R/C Frames Including Changes in Geometry and Non-elastic Behavior under Combined Normal Force and Bending," *Symposium of Resistance and Ultimate Deformability of Structure Acted by Well Defined Repeated Load*, Lisbon, Portugal, 15–22.

Naeim F and Kelly JM (1999), *Design of Seismic Isolated Structures*, Wiley, New York, USA.

Nagarajaiah S, Reinhorn AM and Constantinou MC

(1991), "Nonlinear Dynamic Analysis of 3-D Base-isolated Structures," *Journal of Structural Engineering*, ASCE, **117**(7): 2035–2054.

Okamoto S, Kani N, Higashino M, Koshika N, Kimizuka M, Midorikawa M and Iiba M (2002), "Recent Developments in Seismically Isolated Buildings in Japan," *Earthquake Engineering and Engineering Vibration*, **1**(2): 213–225.

Oliveira F, Morai P and Suleman A (2015), "A Comparative Study of Semi-active Control Strategies for Base Isolated Buildings," *Earthquake Engineering and Engineering Vibration*, **14**(3): 487–502.

OpenSees (2013), *Open System for Earthquake Engineering Simulation*, Computer Program, University of California, Berkeley, California, USA. (Available from: http://opensees.berkeley.edu [15 October 2013]).

Ordonez D, Foti D and Bozzo L (2003), "Comparative Study of the Inelastic Response of Base Isolated Buildings," *Earthquake Engineering and Structural Dynamics*, **32**(1): 151–164.

Ozdemir G and Akyuz U (2012), "Dynamic Analyses of Isolated Structures under Bidirectional Excitations of Near-field Ground Motions," *Shock and Vibration*, **19**(4): 505–513.

Pan P, Zamfirescu DAN, Nakashima M, Nakayasu N and Kashiwa H (2005), "Base-isolation Design Practice in Japan: Introduction to the Post-Kobe Approach," *Journal of Earthquake Engineering*, **9**(1): 147–171.

Panchal VR and Jangid RS (2008), "Seismic Behavior of Variable Frequency Pendulum Isolator," *Earthquake Engineering and Engineering Vibration*, **7**(2): 193–205.

Pant DR, Constantinou MC and Wijeyewickrema AC (2013a), "Re-evaluation of Equivalent Lateral Force Procedure for Prediction of Displacement Demand in Seismically Isolated Structures," *Engineering Structures*, **52**: 455–465.

Pant DR and Wijeyewickrema AC (2013), "Influence of Near-fault Ground Motions on the Response of Base-isolated Reinforced Concrete Buildings Considering Seismic Pounding," *Advances in Structural Engineering*, **16**(12): 1973–1988.

Pant DR and Wijeyewickrema AC (2014), "Performance of Base-isolated Reinforced Concrete Buildings Under Bidirectional Seismic Excitation Considering Pounding with Retaining Walls Including Friction Effects," *Earthquake Engineering and Structural Dynamics*, **43**(10): 1521–1541.

Pant DR, Wijeyewickrema AC and ElGawady MA (2013b), "Appropriate Viscous Damping for Nonlinear Time-history Analysis of Base-isolated Reinforced Concrete Buildings," *Earthquake Engineering and Structural Dynamics*, **42**(15): 2321–2339.

Park R, Priestley MJN and Gill WD (1982), "Ductility of Square-confined Concrete Columns," *Journal of Structural Engineering*, ASCE, **108**(4): 929–950.

Pavlou EA (2005), "Performance of Primary and Secondary Systems in Buildings with Seismic Protective Systems," *PhD Dissertation*, University at Buffalo, State University of New York, NY, USA.

PEER (2013), *Pacific Earthquake Engineering Research Center: Ground Motion Database*, (Available from: http://peer.berkeley.edu/peer_ground_motion_database [21 August 2013]).

Providakis CP (2008a), "Effect of LRB Isolators and Supplemental Viscous Dampers on Seismic Isolated Buildings under Near-fault Excitations," *Engineering Structures*, **30**(5): 1187–1198.

Providakis CP (2008b), "Pushover Analysis of Base-isolated Steel-concrete Composite Structures under Near-fault Excitations," *Soil Dynamics and Earthquake Engineering*, **28**(4): 293–304.

Ribakov Y (2010), "Reduction of Structural Response to Near Fault Earthquakes by Seismic Isolation Columns and Variable Friction Dampers," *Earthquake Engineering and Engineering Vibration*, **9**(1): 113–122.

SAP2000 (2013), *Integrated Finite Element Analysis and Design of Structures*, Version 15, Computers and Structures Inc., Berkeley, CA, USA.

Sayani PJ and Ryan KL (2009), "Comparative Evaluation of Base-isolated and Fixed-base Buildings Using a Comprehensive Response Index," *Journal of Structural Engineering*, ASCE, **135**(6): 698–707.

Skinner RI, Robinson WH and McVerry GH (1993), *An Introduction to Seismic Isolation*, Wiley, Chichester, UK.

Sorace S and Terenzi G (2008), "Analysis and Demonstrative Application of a Base Isolation/ Supplemental Damping Technology," *Earthquake Spectra*, **24**(3), 775–793.

Sorace S and Terenzi G (2014), "Analysis, Design and Construction of a Base-isolated Multiple Building Structure," *Advances in Civil Engineering*, ID 585429, 13p.

Tena-Colunga A and Pérez-Osornio MÁ (2006), "Design Displacements for Base Isolators Considering Bidirectional Seismic Effects," *Earthquake Spectra*, **22**(3): 803–825.

Tsai CS, Chen BJ, Pong WS and Chiang TC (2004), "Interactive Behavior of Structures with Multiple Friction Pendulum Isolation System and Unbounded Foundations," *Advances in Structural Engineering*, **7**(6): 539–551.

Varnava V and Komodromos P (2013), "Assessing the

Effect of Inherent Nonlinearities in the Analysis and Design of a Low-rise Base-isolated Steel Building," *Earthquakes and Structures*, **5**(5): 499–526.

Yassin MHM (1994), "Nonlinear Analysis of Prestressed Concrete Structures under Monotonic and Cyclic Loads," *PhD Dissertation*, University of California, Berkeley, CA, USA.

Ye K, Li L and Zhu H (2009), "A Modified Kelvin Impact Model for Pounding Simulation of Base-isolated Building with Adjacent Structures," *Earthquake Engineering and Engineering Vibration*, **8**(3): 433–446.